Low-Energy Physics Reach of Xenon Detectors for Nuclear-Recoil-Based Dark Matter and Neutrino Experiments

B. G. Lenardo,[1,2,3] J. Xu,[2,*] S. Pereverzev,[2] O. A. Akindele,[2] D. Naim,[3] J. Kingston,[2,†] A. Bernstein,[2] K. Kazkaz,[2] M. Tripathi,[3] C. Awe,[4] L. Li,[4] J. Runge,[4] S. Hedges,[4] P. An,[4] and P. S. Barbeau[4]

[1]*Physics Department, Stanford University, 382 Via Pueblo Mall, Stanford, California 94305, USA*
[2]*Lawrence Livermore National Laboratory, 7000 East Avenue, Livermore, California 94551, USA*
[3]*University of California Davis, Department of Physics, One Shields Avenue, Davis, California 95616, USA*
[4]*Department of Physics, Duke University, and Triangle Universities Nuclear Laboratories, Durham, North Carolina 27710, USA*

(Received 14 June 2019; revised manuscript received 17 September 2019; published 4 December 2019)

Dual-phase xenon detectors lead the search for keV-scale nuclear recoil signals expected from the scattering of weakly interacting massive particle (WIMP) dark matter, and can potentially be used to study the coherent nuclear scattering of MeV-scale neutrinos. New capabilities of such experiments can be enabled by extending their nuclear recoil searches down to the lowest measurable energy. The response of the liquid xenon target medium to nuclear recoils, however, is not well characterized below a few keV, leading to large uncertainties in projected sensitivities. In this work, we report a new measurement of ionization signals from nuclear recoils in liquid xenon down to the lowest energy reported to date. At 0.3 keV, we find that the average recoil produces approximately one ionization electron; this is the first measurement of nuclear recoil signals at the single-ionization-electron level, approaching the physical limit of liquid xenon ionization detectors. We discuss the implications of these measurements on the physics reach of xenon detectors for nuclear-recoil-based WIMP dark matter searches and the detection of coherent elastic neutrino-nucleus scattering.

DOI: 10.1103/PhysRevLett.123.231106

Introduction.—Dual-phase (liquid-gas) xenon time projection chambers (TPCs) are widely used in fundamental physics for the detection of rare low-energy signals. In particular, they have enabled the most sensitive searches for weakly interacting massive particles (WIMPs) [1–3], a class of hypothesized particles which provide a compelling solution to the dark matter problem [4,5]. These experiments search for the keV-scale recoil of a xenon nucleus from WIMP interactions by detecting ionization and scintillation produced in a liquid xenon target. For WIMPs with masses below $\sim 10\ \mathrm{GeV}/c^2$ the recoil spectrum is heavily weighted towards sub-keV energies, but current xenon experiments rapidly lose sensitivity due to the scintillation signals becoming undetectable ($\lesssim 10\%$ efficiency) [6]. On the other hand, the efficiency of detecting ionization electrons can remain $\sim 100\%$ down to the level of single electrons (SEs) thanks to the proportional electroluminescence amplification of the ionization signals in the gas. A few experiments have demonstrated the feasibility of exploring this low energy region via "ionization-only" searches [7–10]. If background in this energy window can be identified and sufficiently mitigated, a significant amount of new parameter space will be opened to xenon-based experiments.

In addition to WIMP dark matter, low energy nuclear recoils can be produced in such a detector via coherent elastic neutrino-nucleus scattering (CEνNS). This interaction was recently measured for the first time in a CsI target [11], and is a subject of interest as a new probe of standard model and beyond-the-standard-model physics [12–16]. In particular, the lowest-energy part of the CEνNS recoil spectrum (<1 keV) is expected to be sensitive to a nonzero neutrino magnetic moment [17]. CEνNS further provides a channel for the flavor-independent detection of solar and supernova neutrinos in the next generation of xenon-based WIMP dark matter detectors [18,19]. Outside of fundamental physics, there is an interest in exploring CEνNS-sensitive instruments for the detection of reactor antineutrinos in nuclear nonproliferation applications [20]. As in the case of low-mass WIMPs, the expected signal from each of these sources has a steeply falling spectrum of nuclear recoils with energies of $\mathcal{O}(1)$ keV and below.

A major technical development needed to enable new low-energy physics reach of xenon-based detectors is a precise calibration of the response to nuclear recoils down to the lowest measurable energy. Dual-phase xenon TPCs are one of the few detector technologies that have demonstrated sensitivity to single charge quanta [21,22], but due to the difficulty of the required measurements, precise nuclear recoil calibrations have only been reported for energies above a few keV [23–29]. In physics analyses studying the sub-keV regime, the energy scale must then be

extrapolated from higher energies and is therefore subject to large uncertainties which propagate directly into projected sensitivities. In this Letter, we address this problem by providing the first measurement of nuclear-recoil-induced ionization in liquid xenon down to the single-electron level, approaching the absolute minimum detectable signal.

The measurements presented in this work simultaneously address three challenges that have prevented previous experiments from fully exploring the low-energy ionization signals in liquid xenon, namely, (a) a nearly 100%-efficient collection of ionization electrons, (b) a high reduction of parasitic electron backgrounds, and (c) a sample of well-defined sub-keV nuclear recoil signals with sensitivity at the single-ionization-electron level. To address the first, we developed a dedicated, compact, and portable xenon TPC and that is capable of measuring extracted electrons with the highest efficiency of any instrument in the literature [30]. To address the second and third, we used neutrons produced by a pulsed, adjustable-energy source, and use an array of liquid scintillator (LS) neutron detectors to tag xenon recoil events. The time-of-flight (TOF) coincidence criteria and pulse-shape discrimination (PSD) capabilities in the LS detectors allow us to reject the otherwise overwhelming background from random coincidences and environmental radiation. We choose the energy of the incident neutrons (∼600 keV) to produce sub-keV recoils at experimentally accessible scattering angles; the LS detector triggered in each event allows precise reconstruction of the nuclear recoil energy.

Data collection and analysis.—Measurements were performed using the tandem accelerator at the Triangle Universities Nuclear Laboratory (TUNL). The setup is illustrated in Fig. 1. A beam of 2.3 MeV protons with a pulse period of 3.2 μs was delivered to a 200 $\mu g/cm^2$ LiF target on a tantalum backing, producing neutrons via the $^7Li(p,n)^7Be$ reaction. A neutron collimator ($56 \times 56 \times 55$ cm) built with a mixture of borated polyethylene and high density polyethylene provided strong absorption of off-axis neutrons, resulting in a 3 cm diameter spot size at the liquid xenon target at the end of the collimator opening. The energy distribution of the forward-going neutrons were measured *in situ* using time of flight, finding a mean energy of 579 ± 3 keV with a 1σ Gaussian spread of 10 keV. Lead shielding (with an opening in the center) placed between the collimator and the xenon detector provided sufficient attenuation of beam-coincident and delayed neutron-capture gammas, and we further included a 6 mm sheet placed completely across the collimator opening to attenuate ^{10}B capture gammas originating near the beam pipe.

The xenon TPC is described in detail in Ref. [30], here we discuss the details most relevant to this work. The liquid xenon target consists of 140 g of liquid xenon ($\varnothing 5 \times 2.5$ cm high), surrounded by a field-shaping cage

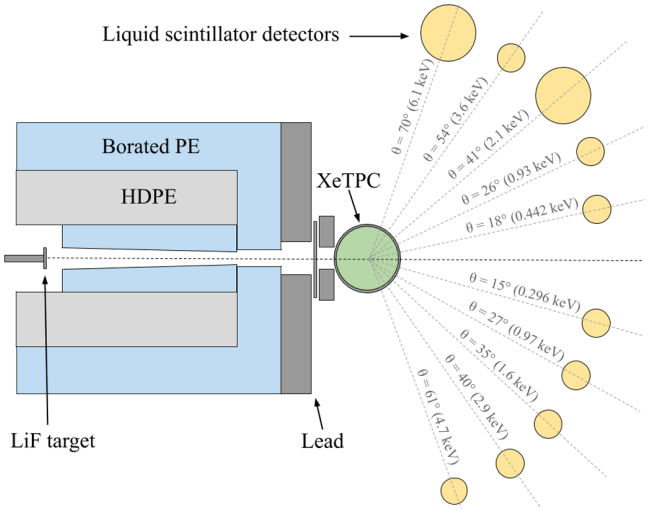

FIG. 1. Diagram of experimental setup (not to scale). The collimator and shielding are color coded to show the borated polyethylene (blue), high-density polyethlyene (light gray), and lead (dark gray). The xenon TPC is shown in green, and the LS backing detectors are shown in yellow. We utilized two sizes for the backing detectors (2 and 4 in. diameter), with relative placements shown here.

which creates two volumes with distinct electric fields: a low-field target volume to drift the ionization electrons towards the liquid surface, and a high-field volume to extract electrons from the liquid surface and produce proportional scintillation light. The light is detected by an array of four 1 in. photomultiplier tubes (Hamamatsu R8520) placed in the gas and a single 2 in. photomultiplier tube (Hamamatsu R8778) placed in the liquid below the cathode. On-beam neutrons entered the xenon TPC through a 0.8 mm-walled, mostly gas-filled PEEK spillover volume which simultaneously fixed the liquid level in the detector and also displaced passive liquid xenon. Outgoing neutrons passed through ∼2.5 cm of passive material before exiting the detector volume. Throughout data acquisition, the temperature and pressure inside the detector were stable to within 0.26 K and 0.021 bar, respectively.

Data were acquired in three separate measurement campaigns with drift fields of 220 V/cm, 550 V/cm, and 2.2 kV/cm applied across the target volume. Each acquisition lasted approximately two days. A fourth drift field dataset is obtained by selecting events from all three acquisitions with nuclear recoils in the high-field extraction volume that contained a combined event count comparable to the other three configurations. The full dataset contains 3.6×10^7 triggered events.

The single-electron (SE) response of the detector was calibrated using posttrigger pulses, which arise from delayed electron emission and photoionization; we measured an average of 56.5 ± 0.3 photoelectrons (PE) per extracted electron with a 1σ width of 11.6 ± 0.3 PE. To calibrate signal collection efficiency, we measured an

electron lifetime in the liquid xenon of 232^{+294}_{-82} μs [31]. This results in an average signal attenuation of ∼3% due to electron attachment on dissolved impurities. At the operating extraction field of 6.2 kV/cm in the liquid, the efficiency of extracting an ionization electron into the gas is estimated to be $95.5^{+1.4}_{-1.7}$% using the extraction efficiency measured previously in the xenon TPC employed here [30].

Scattered neutrons were tagged by one of ten LS neutron detectors positioned in an arc with radius ∼60 cm, spanning scattering angles of 15–70° (corresponding to nuclear recoils between 0.30 and 6.1 keV). Data acquisition was triggered by a pulse in the liquid xenon detector within a coincidence window of 25 μs after a pulse in one of the LS channels (40 μs for a subset of the data). A 3 ms veto was applied following high-energy ($\gtrsim$10 keV) events, which are known to produce an elevated single-electron background rate in dual-phase xenon TPCs that decays at the ms timescale [22,32]. The trigger efficiency for signals in the TPC was evaluated using dedicated measurements of xenon TPC pulses that followed the main triggering pulses in acquired events [31]. We measure an efficiency of 97.5 ± 0.1% for single-electron signals and ∼100% for larger signals. For each valid trigger, 16 waveforms were digitized: five PMT channels from the xenon TPC, ten LS channels, and the beam pulse monitor (BPM), which measured the proton-on-target time from the accelerator.

We compute the neutron TOF as the time delay between the LS pulse and the preceding BPM pulse. We select only the events within the full width at half maximum (FWHM) of the neutron TOF peak, to suppress both beam-produced and random-coincidence gamma background [31]. Simulations indicate that this cut removes ∼75% of multiple-scatter background events (in which neutrons scatter a second time in passive materials), while retaining ∼70% of the single-scatter events. We then use the PSD capabilities of the LS to remove residual gamma coincidence background.

In the TPC, ionization pulses are separated from liquid xenon scintillation pulses by their pulse width. We then require the position of a candidate event, measured using the light distribution in the top PMT array, to be within 1.3 cm of the center of the detector where the SE response is highly uniform. An additional cut is applied on the asymmetry of light in the top vs bottom PMT channels to amend the position reconstruction with a four-pixel readout [33]. This cut is chosen to be ∼1.4σ below the peak top-bottom asymmetry (TBA) value for SEs, resulting in an acceptance of 92%; for multielectron pulses with narrower TBA distributions, the acceptance increases to $\gtrsim$98%.

We observe a non-negligible rate of random coincidence SE background in the TPC after all cuts. This background produces events with a nonphysical charge drift time, calculated here as the time delay between the prompt LS pulse and the ionization pulse in the xenon TPC. The drift times of neutron-induced ionization events are bounded by the physical extent of the target volume and are $\lesssim$15 μs, but random coincidence events can produce larger drift time values. The measured spectrum and rate of events in the nonphysical drift region is extrapolated into the signal drift time region to infer the background contamination, which is then subtracted from the measured ionization spectrum [31].

Experimental results.—Figure 2 shows the background-subtracted and efficiency-corrected ionization signals from xenon nuclear recoils of 932, 442, and 296 eV, the three lowest-energy channels in this measurement. In the 932 eV spectrum, the peak observed at 5–6e^- is attributed to single scatter neutron interactions in the xenon TPC. The increased uncertainty around single-electron signals is a result of the aforementioned background subtraction. In the 442 and 296 eV xenon recoil spectra, we observe distinct single-, double-, triple-electron peaks, which demonstrate unprecedented ionization signal resolution at such low energies in a dual-phase xenon detector.

Each spectrum is fitted with a modeled spectrum to extract the average number of ionized electrons. The model is based on a Geant4 simulation and uses either a Gaussian (for spectra above 900 eV, where a two-sided peak is observed) or a Poisson distribution (for the two lowest energies, 442 and 296 eV) to generate an electron number

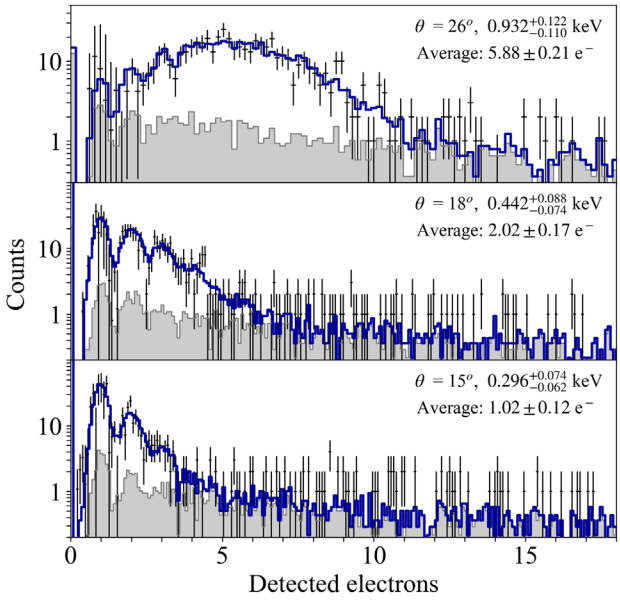

FIG. 2. Background-subtracted and efficiency-corrected nuclear recoil ionization spectra measured at a drift field of 220 V/cm (black), at the three lowest energies explored in this work. We clearly observe quantized single-, double-, and triple-electron signals. The spectra in each channel are fitted with simulated spectra (blue), which include the expected neutron multiple-scattering background (gray), allowing us to extract the average number of ionization electrons as a function of recoil energy. We show the scattering angle, the mean and central 68 percentile of the simulated nuclear recoil energy distribution, and the average number of ionized electrons obtained from the fit.

distribution, which is then resampled to model the effects of electron capture on impurities in the bulk and incomplete electron extraction at the liquid surface. The occupancy of zero-electron events, which is not measured due to our trigger requirements, is inferred by the estimated total event rate based on interaction cross section in the Geant4 simulation. Uncertainty in the predicted rate results in a systematic uncertainty of 6% in the average ionization signal for the two lowest-energy channels. A model-independent estimation of the zero-rate and ionization yield in these channels, derived by simply counting events in the measurements compared to simulations, agrees with the Poisson-based fits within the statistical uncertainties, but deviates by 5.5% at 442 and 11.0% at 296 eV. We use the Poisson fit results to enable the simulation of low energy signals below, and take the deviation from the model-independent estimation as a measure of our systematic uncertainty due to the choice of model. Two further sources of systematic error arise from the uncertainties in the electron extraction efficiency and the electron lifetime, which each contribute ∼2% scaling uncertainties across all energy channels.

Figure 3 shows the average numbers of ionization electrons evaluated as a function of xenon recoil energy for the lowest and highest drift electric field values in this experiment [31]. Our measurements at 220 V/cm electric field agree with LUX (180 V/cm), and substantially improve the precision at low energies. Below 2 keV, we measure a significantly lower ionization yield than that predicted by the widely used NESTv2.0 simulation package [34], which is tuned to match previously published data [23–27,35] and is driven by the LUX measurements at low energies [36]. We fit a second-order polynomial fit to our measurement of the ionization yield vs energy as an empirical model (shown in Fig. 3), which we use in the sensitivity estimates described below. While this fit predicts a yield of 0 electrons below 180 ± 40 eV nuclear recoil energy, we emphasize that this is an empirical extrapolation and not a direct measurement of a threshold for ionization in liquid xenon. Such a threshold is not typically included in models of charge production in liquid xenon [37–39], but has been suggested [40]. This extrapolation is only ∼100 eV below the mean nuclear recoil energy in our smallest-angle channel, and is comparable to the spread of recoil energies observed by this channel; it is therefore a reasonably conservative extrapolation. In addition, because the average signals in this extrapolation region are smaller than a single electron, while realistic experiments will likely require two or more detected electrons to remove spurious background, this does not introduce a large uncertainty in predictions of experimental sensitivities.

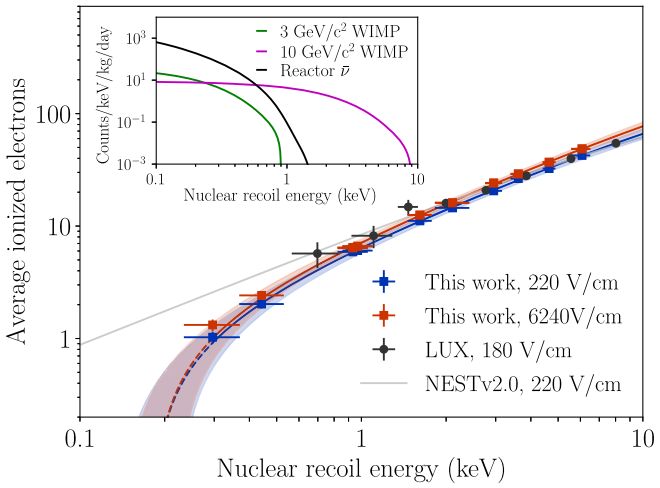

FIG. 3. Average number of ionization electrons produced in liquid xenon as a function of nuclear recoil energy (using electron extraction efficiency values measured in Ref. [30]). For comparison, we show measurements from the LUX dark matter experiment [28], as well as the prediction from the NEST simulation package [34], which is based on evaluations of published data [23–27,35,36] and is driven by the LUX measurements at low energies. The inset shows the expected recoil spectra from reactor antineutrinos CEνNS and dark matter WIMP models with different masses for comparison. Here we assume the standard halo model (Ref. [41]) and a spin-independent interaction cross section (denoted σ_0) of 10^{-41} cm^2 for the WIMP spectra, and use the parametrizations in Ref. [42] for the reactor antineutrino emission spectrum.

As shown in Fig. 3 the average number of ionized electrons at each recoil energy increases by approximately ∼15% if the applied field is increased from 200 to 6240 V/cm. Our maximum of 6240 V/cm is the highest applied electric field studied in a nuclear recoil measurement, and is significantly higher than planned next-generation experiments [18,43]. This work therefore reports the maximum number of electrons that may be detected at low energies in dual-phase xenon experiments for the foreseeable future.

Impact on the projected physics reach of xenon ionization detectors.—Using the polynomial fit to the data at 6240 V/cm, we can create robust predictions of the expected ionization spectra from WIMP dark matter or CEνNS. Examples are shown in Fig. 4 (left). This enables us to estimate the potential sensitivity of an optimized xenon ionization detector to low-mass WIMP interactions in the standard halo model [41]. Figure 4 (right) shows the expected sensitivity of an experiment with a threshold at $2e^-$, with a background-free exposure of 10 kg yr. Current xenon experiments have met such background goals for signals above $10e^-$, but achieving this background level down to $2e^-$ signals requires that the pathological few-electron backgrounds observed in existing experiments be adequately addressed. Here we assume a $2e^-$ threshold to allow limited SE background to be present. For exposures larger than 10 kg yr, residual radioactivity (at present levels) and solar neutrino CEνNS interactions would become limiting backgrounds and the sensitivity will not increase proportionally with the exposure.

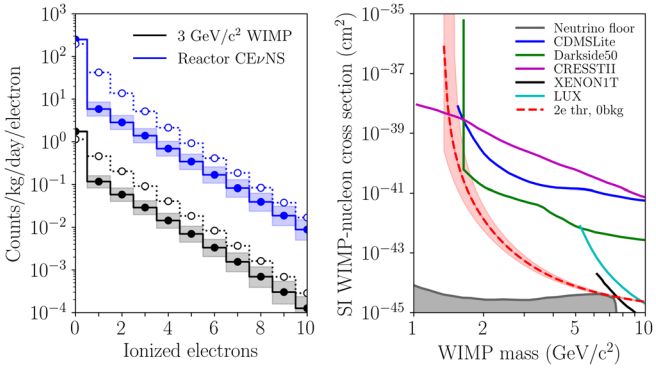

FIG. 4. *Left*—Projected ionization spectra from a 3 GeV/c^2 WIMP (assuming $\sigma_0 = 10^{-41}$ cm^2) and reactor antineutrino coherent scattering. Projections calibrated by the measurements in this work (solid lines) deviate significantly from those using NESTv2.0 (dashed), which is tuned to fit existing data. *Right*—Projected sensitivity of a background-free, ionization-only search for low-mass WIMP dark matter (dashed red). The assumed exposure is 10 kg yr. Solid lines show existing limits from CDMSLite [44], Darkside50 [45], CRESSTII [46], XENON1T [2], and LUX [1] for comparison. Uncertainty bands in both the spectra and projected limits are calculated by propagating the uncertainties in the second-order polynomial fit parameters.

On the possibility of using xenon detectors for the detection of MeV-scale neutrinos, this work is the first to probe the relevant energy region to the expected CEνNS signal from reactor antineutrinos in xenon; 99.9% of such events produce nuclear recoils below the previous lowest measurement of 0.7 keV. The definitive measurement of nonzero ionization electrons in this energy region indicates that xenon TPCs are indeed sensitive to nuclear recoils from reactor antineutrinos, and that the primary challenge faced by such experiments will be achieving the necessary reduction of backgrounds in an above-ground environment. A projected reactor CEνNS rate spectrum using the ionization yield from this work is shown in Fig. 4 (left), assuming a detector placed 25 m from a 3GW$_{\text{th}}$ reactor core. For CEνNS interaction of xenon with higher-energy neutrinos (from the Spallation Neutron Source, for example) that primarily produce nuclear recoils above a few keV, this calibration may have an impact in searches for a nonzero neutrino magnetic moment [17].

This project is supported by the U.S. Department of Energy (DOE) Office of Science, Office of High Energy Physics under Work Proposals No. SCW1508 and No. SCW1077 awarded to Lawrence Livermore National Laboratory (LLNL). LLNL is operated by Lawrence Livermore National Security, LLC, for the DOE, National Nuclear Security Administration (NNSA) under Contract No. DE-AC52-07NA27344. Certain equipment used in this measurement was recycled from the LLNL DUS Second Time Around store. TUNL is operated as a DOE Center of Excellence under Grant No. DE-FG02-97ER41033. D. N. is supported by the DOE/NNSA under Award No. DE-NA0000979 through the Nuclear Science and Security Consortium. Duke University student support is provided by the DOE under Award No. DE-SC0014249. We thank Sean Durham and Jesse Hamblen from LLNL, and Dave Hemer, Keith Delong, and Michael Irving from UC Davis for their technical support on designing and constructing the xenon TPC detector. We also thank Vladimir Mozin and Phillip Kerr for their help during early tests, the TUNL scientific and technical staff for their assistance during setup and operation, and Professor John Mattingly of North Carolina State University for lending us the LS detectors used in this work. Finally, we thank the members of the LUX and LZ Collaborations for their constructive discussions on this measurement and possible implications.

*Corresponding author.
xu12@llnl.gov
†Present address: The University of Chicago, Division of the Physical Sciences, 5801 South Ellis Avenue, Chicago, Illinois 60637, USA.

[1] D. S. Akerib *et al.* (LUX Collaboration), Phys. Rev. Lett. **118**, 021303 (2017).
[2] E. Aprile *et al.* (XENON Collaboration), Phys. Rev. Lett. **121**, 111302 (2018).
[3] A. Tan *et al.* (PandaX-II Collaboration), Phys. Rev. Lett. **117**, 121303 (2016).
[4] G. Jungman, M. Kamionkowski, and K. Griest, Phys. Rep. **267**, 195 (1996).
[5] M. W. Goodman and E. Witten, Phys. Rev. D **31**, 3059 (1985).
[6] D. S. Akerib *et al.* (LUX Collaboration), Phys. Rev. Lett. **116**, 161301 (2016).
[7] R. Essig, A. Manalaysay, J. Mardon, P. Sorensen, and T. Volansky, Phys. Rev. Lett. **109**, 021301 (2012).
[8] J. Angle *et al.* (XENON10 Collaboration), Phys. Rev. Lett. **107**, 051301 (2011).
[9] E. Aprile *et al.* (XENON Collaboration), Phys. Rev. D **94**, 092001 (2016).
[10] E. Aprile *et al.* (XENON Collaboration), arXiv:1907.11485.
[11] D. Akimov *et al.*, Science **357**, 1123 (2017).
[12] B. Dutta, R. Mahapatra, L. E. Strigari, and J. W. Walker, Phys. Rev. D **93**, 013015 (2016).
[13] B. Dutta, Y. Gao, A. Kubik, R. Mahapatra, N. Mirabolfathi, L. E. Strigari, J. W. Walker, Phys. Rev. D **94**, 093002 (2016).
[14] A. J. Anderson, J. M. Conrad, E. Figueroa-Feliciano, C. Ignarra, G. Karagiorgi, K. Scholberg, M. H. Shaevitz, and J. Spitz, Phys. Rev. D **86**, 013004 (2012).
[15] M. Cadeddu, C. Giunti, K. A. Kouzakov, Y. F. Li, A. I. Studenikin, and Y. Y. Zhang, Phys. Rev. D **98**, 113010 (2018).
[16] B. Cañas, E. A. Garcés, O. G. Miranda, and A. Parada, Phys. Lett. B **784**, 159 (2018).
[17] K. Scholberg, Phys. Rev. D **73**, 033005 (2006).

[18] D. S. Akerib *et al.* (LUX-ZEPLIN Collaboration), arXiv: 1802.06039.
[19] R. F. Lang, C. McCabe, S. Reichard, M. Selvi, and I. Tamborra, Phys. Rev. D **94**, 103009 (2016).
[20] C. Hagmann *et al.*, IEEE Trans. Nucl. Sci. **51**, 2151 (2004).
[21] B. Edwards *et al.*, Astropart. Phys. **30**, 54 (2008).
[22] E. Aprile *et al.*, J. Phys. G **41**, 035201 (2014).
[23] E. Aprile, C. E. Dahl, L. de Viveiros, R. J. Gaitskell, K. L. Giboni, J. Kwong, P. Majewski, K. Ni, T. Shutt, and M. Yamashita, Phys. Rev. Lett. **97**, 081302 (2006).
[24] M. Horn *et al.*, Phys. Lett. B **705**, 471 (2011).
[25] P. Sorensen *et al.*, Nucl. Instrum. Methods Phys. Res., Sect. A **601**, 339 (2009).
[26] E. Aprile *et al.* (XENON100 Collaboration), Phys. Rev. D **88**, 012006 (2013).
[27] A. Manzur, A. Curioni, L. Kastens, D. N. McKinsey, K. Ni, and T. Wongjirad, Phys. Rev. C **81**, 025808 (2010).
[28] D. S. Akerib *et al.* (LUX Collaboration), arXiv:1608.05381 [Phys. Rev. C (to be published)].
[29] E. Aprile, M. Anthony, Q. Lin, Z. Greene, P. de Perio, F. Gao, J. Howlett, G. Plante, Y. Zhang, and T. Zhu, Phys. Rev. D **98**, 112003 (2018).
[30] J. Xu, S. Pereverzev, B. Lenardo, J. Kingston, D. Naim, A. Bernstein, K. Kazkaz, and M. Tripathi, Phys. Rev. D **99**, 103024 (2019).
[31] See Supplemental Material at http://link.aps.org/supplemental/10.1103/PhysRevLett.123.231106 for technical analysis discussions and full data release.
[32] P. Sorensen and K. Kamdin, J. Instrum. **13**, P02032 (2018).
[33] S. Stephenson *et al.*, J. Instrum. **10**, P10040 (2015).
[34] M. Szydagis *et al.*, Noble Element Simulation Technique v2.0, https://doi.org/10.5281/zenodo.1314669(2018).
[35] P. Sorensen, J. Cosmol. Astropart. Phys. 09 (2010) 033.
[36] D. S. Akerib *et al.* (LUX Collaboration), Phys. Rev. Lett. **116**, 161301 (2016).
[37] J. Lindhard, V. Nielsen, M. Scharff, and P. V. Thomsen, Mat. Fys. Medd. K. Dan. Vidensk. Selsk **33**, 10 (1963).
[38] F. Bezrukov, F. Kahlhoefer, and M. Lindner, Astropart. Phys. **35**, 119 (2011).
[39] B. Lenardo, K. Kazkaz, A. Manalaysay, J. Mock, M. Szydagis, and M. Tripathi, IEEE Trans. Nucl. Sci. **62**, 3387 (2015).
[40] P. Sorensen, Phys. Rev. D **91**, 083509 (2015).
[41] J. Lewin *et al.*, Astropart. Phys. **6**, 87 (1996).
[42] P. Huber, Phys. Rev. C **84**, 024617 (2011).
[43] E. Aprile *et al.*, J. Cosmol. Astropart. Phys. 04 (2016) 027.
[44] R. Agnese *et al.* (SuperCDMS Collaboration), Phys. Rev. Lett. **112**, 041302 (2014).
[45] P. Agnes *et al.* (DarkSide Collaboration), Phys. Rev. Lett. **121**, 081307 (2018).
[46] G. Angloher *et al.*, Eur. Phys. J. C **72**, 1971 (2012).